






# Parallel Electron Heating by Tangential Discontinuity in the Turbulent Magnetosheath

Y. Y. Liu<sup>1</sup>, H. S. Fu<sup>1</sup> , C. M. Liu<sup>1</sup> , Z. Wang<sup>1</sup> , P. Escoubet<sup>2</sup>, K.-J. Hwang<sup>3</sup>, J. L. Burch<sup>3</sup>, and B. L. Giles<sup>4</sup>

<sup>1</sup>School of Space and Environment, Beihang University, Beijing, People's Republic of China; [huishanf@gmail.com](mailto:huishanf@gmail.com)

<sup>2</sup>Space Science Department, European Space Agency, Noordwijk, The Netherlands

<sup>3</sup>Southwest Research Institute, San Antonio, TX, USA

<sup>4</sup>NASA Goddard Space Flight Center, Greenbelt, MD, USA

Received 2019 March 9; revised 2019 May 7; accepted 2019 May 8; published 2019 May 24

## Abstract

Energetic electrons exist widely in the turbulent magnetosheath, but how they are generated remains unclear. Here we report a new structure, at which electrons are efficiently accelerated in the direction parallel to the magnetic field. Such a structure, formed at the edge of a high-speed jet (HSJ), is a tangential discontinuity (TD) in the MHD regime, but exhibits impulsive fine structures in the kinetic-scale regime. The pulsation of the TD, caused by time-varying size of the HSJ, leads to the energization process: when the transverse section of the HSJ increases, a magnetic mirror is formed and subsequently electrons are trapped and accelerated via the Fermi mechanism; when the transverse section of the HSJ decreases, the magnetic mirror disappears and subsequently electrons escape. Such parallel electron heating can lead to three times of parallel-temperature increase; it can shed light on the study of electron heating in the solar wind, where TDs exist extensively.

*Key words:* acceleration of particles – magnetic reconnection – solar wind – turbulence

## 1. Introduction

Energetic electrons exist extensively in the turbulent magnetosheath (Chasapis et al. 2015; Cohen et al. 2016). These electrons, with energy from a few times the thermal energy to hundreds of kiloelectron volts, can have pitch angle distribution (PAD) in the “cigar,” “pancake,” “isotropic,” “butterfly,” and “rolling-pin” shapes (Fu et al. 2012c; Liu et al. 2017a, 2017b; Zhao et al. 2019); they play a significant role in the flux transport in the near-Earth space (Duan et al. 2014; Gabrielse et al. 2014; Turner et al. 2015; Xu et al. 2018). Also, they can damage spacecraft, injure astronauts, and consequently produce a dangerous space environment. Understanding the generation of these electrons, therefore, is an important topic in plasma physics and astrophysics.

So far, how these electrons are generated in the turbulent magnetosheath has been poorly understood, owing to the scarcity of high-resolution measurements. In previous studies, a few processes or structures were suggested. For example, the magnetic reconnection occurring in the thin current sheet in the turbulent magnetosheath (Retinò et al. 2007; Sundkvist et al. 2007; Eriksson et al. 2016, 2018; Yordanova et al. 2016; Peng et al. 2017; Chen et al. 2018; Phan et al. 2018) could energize electrons via the Fermi or betatron mechanisms (Drake et al. 2006; Fu et al. 2011b, 2013b, 2019c; Hoshino 2012; Guo et al. 2014a; Matsumoto et al. 2015; Liu et al. 2017c; Liu & Fu 2019); the shock, which appears as a boundary separating the magnetosheath from the solar wind (known as bow shock) or a boundary separating the fast solar wind from the slow solar wind (known as interplanetary shock Zong et al. 2009, 2012; Fu et al. 2011a, 2012a, 2012b), could energize electrons via the convection electron field (in front of a quasi-perpendicular shock; Peng et al. 2015; Johlander et al. 2016) or the Fermi mechanism (in front of a quasi-parallel shock; Guo et al. 2014b; Park et al. 2015; Zank et al. 2015); the Joule heating happening in the current filaments could energize electrons through kinetic-scale turbulence (Wan et al. 2012; Chasapis et al. 2015, 2017; Fu et al. 2017; Liu et al. 2018a, 2018b); the wave-particle interaction, which exists widely in the

magnetosheath could energize electrons through cyclotron resonance (Cairns & McMillan 2005; Wilson et al. 2013; Agapitov et al. 2014; Hughes et al. 2014; Cao et al. 2017; Oka et al. 2017; Fu et al. 2019b), etc. These structures/processes can explain the electron energization in the turbulent magnetosheath.

Here we report a new type of magnetic structure responsible for electron energization in turbulent plasmas. This structure, formed at the edge of a high-speed jet (HSJ), is a tangential discontinuity (TD) in the MHD regime, but exhibits impulsive fine structures in the kinetic-scale regime; it can energize electrons to achieve three times of temperature increase. We propose a model, based on time-varying size of the HSJ, to explain such energization.

## 2. Observations

The *MMS* mission (Burch et al. 2016), crossing the Earth's magnetosheath frequently with high-resolution measurements of particles, provides a good opportunity to address this issue. In this study, we use the *MMS* data, particularly data from the FluxGate Magnetometer (FGM) (Russell et al. 2016), Fast Plasma Investigation instrument (Pollock et al. 2016), and the Electric Double Probes (EDP; Torbert et al. 2016). To know the solar wind condition, we also use the *ACE* data collected at the L1 point. All these data were originally prescribed in Geocentric Solar Ecliptic (GSE) coordinates.

The event of interest was detected by *MMS* on 2015 November 16, at 12:05–12:22 UT, when *MMS* was located in the magnetosheath at (10.2, 4.6, −0.9)  $R_E$  with very small separations (Figure 1(a)); it observed electrons with energy of ~60 eV (Figure 1(l)), which is the typical energy of the magnetosheath population. Since spacecraft separation was small (<20 km, not shown), the four *MMS* spacecraft measured similar magnetic field and plasma properties. For simplicity, we only show the measurements of *MMS* 1 in this study.

Figure 1(b) presents the interplanetary magnetic field (IMF)  $B_Z$  measured by *ACE* at the L1 point. Such component ( $B_Z$ )

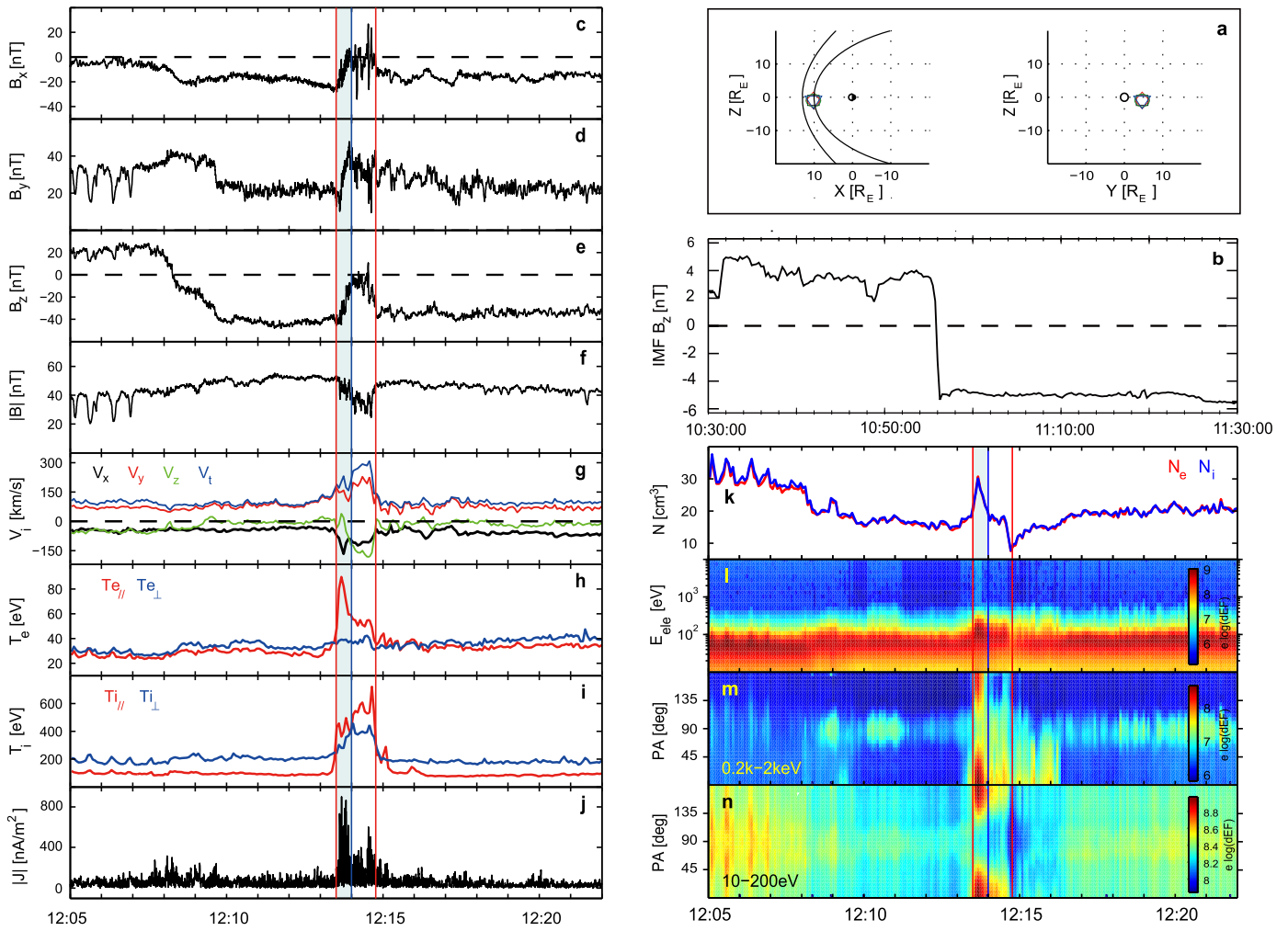


**Figure 1.** MMS observations of a high-speed jet in the magnetosheath on 2015 November 16. (a) The position of MMS; (b) the IMF  $B_z$  component; (c)–(f) the three components and magnitude of magnetic field; (g) the ion bulk velocity; (h)–(i) the electron and ion temperatures; (j) the current density resolved by the Curlmeter technique; (k) the plasma density; (l) the electron energy spectrum; (m)–(n) the pitch angle distribution of the 0.2–2 and 0.01–0.2 keV electrons. GSE coordinates are used.

reversed from northward (+4 nT) to southward (−5 nT) at 10:53:00 UT. Seventy-five minutes later, at ~12:08:00 UT, MMS 1 detected a similar reversal of  $B_z$  from northward (+20 nT) to southward (−40 nT) in the magnetosheath (Figure 1(e)), indicating a propagation of such reversal from the L1 point to the magnetosheath. After the  $B_z$  reversal, magnetic field in the magnetosheath is weakly fluctuating (see Figures 1(c)–(e)) except at 12:13:25–12:14:50 UT (see the two vertical red lines), when magnetic field (Figures 1(c)–(e)), electron and ion temperatures (Figures 1(h)–(i)), and ion flow velocity (Figure 1(g)) dramatically change. Such change should be attributed to a local structure encountered by the MMS spacecraft, rather than a remote structure propagating from the solar wind, because the *ACE* spacecraft did not observe considerable variations of magnetic field after the  $B_z$  reversal (see Figure 1(b)). Inside this structure, the flow velocity (Figure 1(g)) is  $308 \times (-0.24 \ 0.78 - 0.58) \text{ km s}^{-1}$ , significantly larger than the flow velocity in the background magnetosheath  $123 \times (-0.44 \ 0.89 \ 0.12) \text{ km s}^{-1}$ , and thus can be termed HSJ. Such HSJ has been widely reported in the magnetosheath (Amata et al. 2011; Dmitriev & Suvorova 2012; Plaschke et al. 2013; Eriksson et al. 2016; Han et al. 2017; Palmroth et al. 2018; Wang et al. 2018), and is possibly

facilitating magnetic reconnection (Hietala et al. 2009, 2018). Inside the HSJ, the magnetic field is weak (Figure 1(f)) and the ion and electron temperatures are high (Figures 1(h)–(i)). Both the HSJ and background flow are primarily along the  $Y_{\text{GSE}}$  direction but still there is an angle  $43^\circ$  between them. The leading edge of this HSJ, characterized by a sharp increase of current density during 12:13:25–12:14:00 UT (Figure 1(j), see the vertical gray shade), is particularly interesting and will be studied in detail in this paper.

Figure 2 analyzes the properties of this edge, including the magnetic field and ion flow velocity in GSE coordinates (Figures 2(b) and (d)), plasma density (Figure 2(f)), and thermal and magnetic pressures (Figure 2(g)). We also transform the magnetic field and ion velocity data to the local magnetic normal coordinates (LMN; Figures 2(c) and (e)), which are determined by the minimum variance analysis of the magnetic field (Fu et al. 2012d, 2019a) during crossing of the HSJ edge. Here  $L$  corresponds to the maximum variance component,  $N$  coincides with the normal of the edge, and  $M$  completes the right-hand coordinate system. Relative to the GSE coordinate,  $L = (0.51, 0.42, 0.75)$ ,  $M = (-0.30, 0.90, -0.30)$ , and  $N = (0.80, 0.07, -0.59)$ . At the entrance of this edge (12:13:25 UT, left vertical dashed line), the plasma and

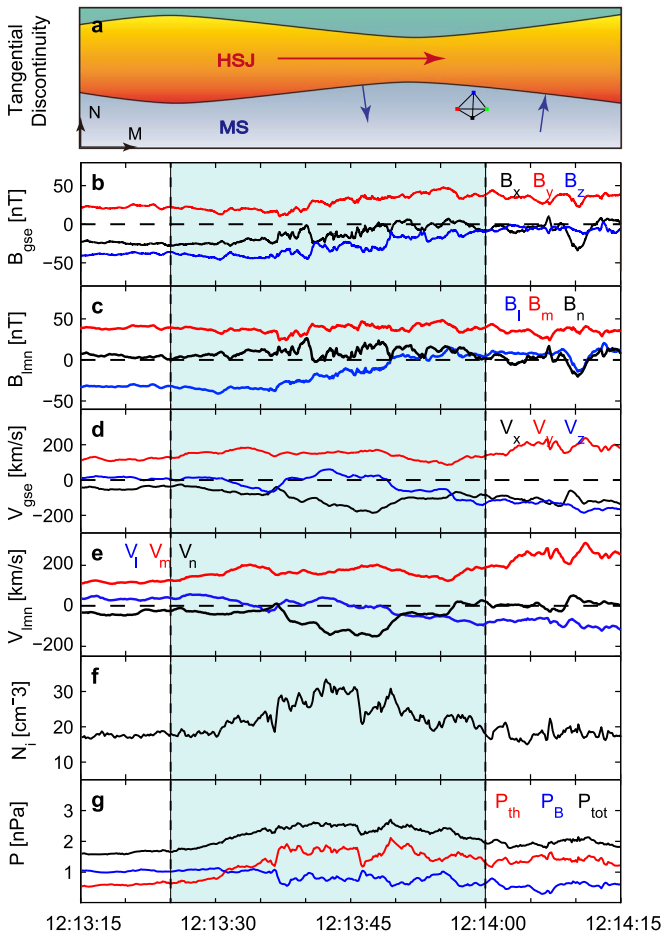


**Figure 2.** Properties of the edge of the high-speed jet. (a) A schematic illustrating this edge; (b)–(c) the three components of magnetic field in GSE and LMN coordinates; (d)–(e) the three components of ion bulk velocity in GSE and LMN coordinates; (f) the plasma density; (g) the thermal, magnetic, and total pressures.

magnetic parameters are  $B_{L1} \approx -31$  nT,  $B_{M1} \approx 37$  nT,  $B_{N1} \approx 1$  nT,  $V_{L1} \approx 45$  km s<sup>-1</sup>,  $V_{M1} \approx 124$  km s<sup>-1</sup>,  $V_{N1} \approx -8$  km s<sup>-1</sup>,  $N_{11} \approx 18$  cm<sup>-3</sup>, and  $P_{tot1} \approx 1.7$  nPa; while at the exit of this edge (12:14:00 UT, right vertical dashed line), they are  $B_{L2} \approx 4$  nT,  $B_{M2} \approx 42$  nT,  $B_{N2} \approx 2$  nT,  $V_{L2} \approx -101$  km s<sup>-1</sup>,  $V_{M2} \approx 187$  km s<sup>-1</sup>,  $V_{N2} \approx 8$  km s<sup>-1</sup>,  $N_{12} \approx 18$  cm<sup>-3</sup>, and  $P_{tot2} \approx 1.9$  nPa. Clearly, across this edge (from 12:13:25 UT to 12:14:00 UT), the tangential magnetic field and velocity changed dramatically ( $|\delta B_L| \approx 35$  nT,  $|\delta V_L| \approx 146$  km s<sup>-1</sup>), while their normal components were very small ( $|B_N| < 2$  nT,  $|V_N| < 8$  km s<sup>-1</sup>). These features meet the criteria of TD, and thus we can identify this edge (vertical shade) as a TD in the MHD regime—without consideration of the interior of this structure. Moreover, having known the vertical direction of the TD, we can estimate its thickness as  $\sim 980$  km by multiplying the background flow speed in the magnetosheath ( $V_N \approx 28$  km s<sup>-1</sup>) and the duration of the structure ( $\sim 35$  s). Considering the local ion inertial length  $d_i = c/\omega_{pi} \approx 56.9$  km, such thickness of the TD ( $\sim 980$  km) is about  $17 d_i$ .

Such TD, interestingly, had a back-and-forth motion in the  $N$  direction according to timing analyses (see also the high-resolution data in Figure 4(d)), meaning that the HSJ wrapped by this TD may have time-varying size in the transverse section. Such time-varying HSJ can be produced by

perturbations in the magnetosheath (Hietala et al. 2009) or unsteady magnetic reconnection (Fu et al. 2013a). Figure 2(a) is a cartoon illustrating the shape of this TD. The TD (see the black lines) forms at the edge of the HSJ (the orange area) propagating in the background magnetosheath. Since the HSJ has time-varying size in the transverse section, the back-and-forth motion of TD in the  $N$  direction (see the blue arrows) could be observed by the MMS spacecraft (see the tetrahedron).

Interestingly, we find particle heating around this TD. Figures 1(h)–(i) present measurements of the electron and ion temperature. As can be seen, during crossing of the HSJ (from 12:13:25 to 12:14:50 UT, between the two vertical red lines), both electron and ion temperatures increase significantly (Figures 1(h)–(i)). The increase of ion temperature happens in both the parallel (red line) and perpendicular (blue line) directions and covers the whole HSJ from 12:13:25 to 12:14:50 UT (Figure 1(i)). There is a nice correlation between the ion temperature (Figure 1(i)) and ion flow velocity (Figure 1(g)), meaning that these hot ions are transported from other places along with the HSJ. Heating of these ions should occur near the source of the HSJ, which is far away, but does not occur locally. The increase of electron temperature exhibits quite different features from ions. In particular, we find electron temperature increase only in the parallel direction (red line, see Figure 1(h)) but not in the perpendicular direction (blue line, see Figure 1(h)). Such parallel heating, leading to three times of temperature increase (from 30 to 90 eV), occurs primarily at the leading edge of the HSJ (Figure 1(h), see the vertical shade), i.e., associated with the TD. It shows no correlation with the ion flow velocity (Figure 1(g)), indicating that these electrons are heated locally, but not transported from other places. Such local parallel energization appears over a wide energy range from 60 to 600 eV (Figure 1(l)); it produces a “cigar” distribution (Fu et al. 2012c; Liu et al. 2017a), which exhibits electron pitch angles primarily in the parallel and antiparallel directions (see Figures 1(m)–(n)).

Figure 3 presents phase space densities (PSDs) of the heated electrons, detected inside the edge at 12:13:37.3 UT (see Figure 3(a) and the red diamonds in Figures 3(b)–(d)), as well as PSDs of the background population, detected in the magnetosheath at 12:13:36.6 UT (see the blue squares in Figures 3(b)–(d)), which can be treated as the source of energization, because the electron heating in this event is a local process. These two populations (heated electrons and source) are also marked by the two arrows at the bottom of Figure 4. As can be seen, in the magnetosheath (at 12:13:36.6 UT), electron PADs are isotropic (Figures 4(e)–(f)), while inside the edge (at 12:13:37.3 UT), electron PADs are “cigar-type,” with more electrons in the parallel and antiparallel directions (Figures 4(e)–(f)). Such a “cigar-type” distribution can appear from 60 to 600 eV (Figure 3(a)) but is most prominent at 120 eV, where the parallel PSD is 20 times higher than the perpendicular PSD (see Figure 3(a)). We use the Maxwellian distribution to fit the omnidirectional PSDs of these two populations and find that the distribution function at 12:13:37.3 UT (Figure 3(b), see red line) is much wider than the distribution function at 12:13:36.6 UT (Figure 3(b), see blue line), meaning that the electron heating indeed happens. When specifically comparing these two populations in the parallel and perpendicular directions (Figures 3(c)–(d)), interestingly, we find that the electron heating only happens in the

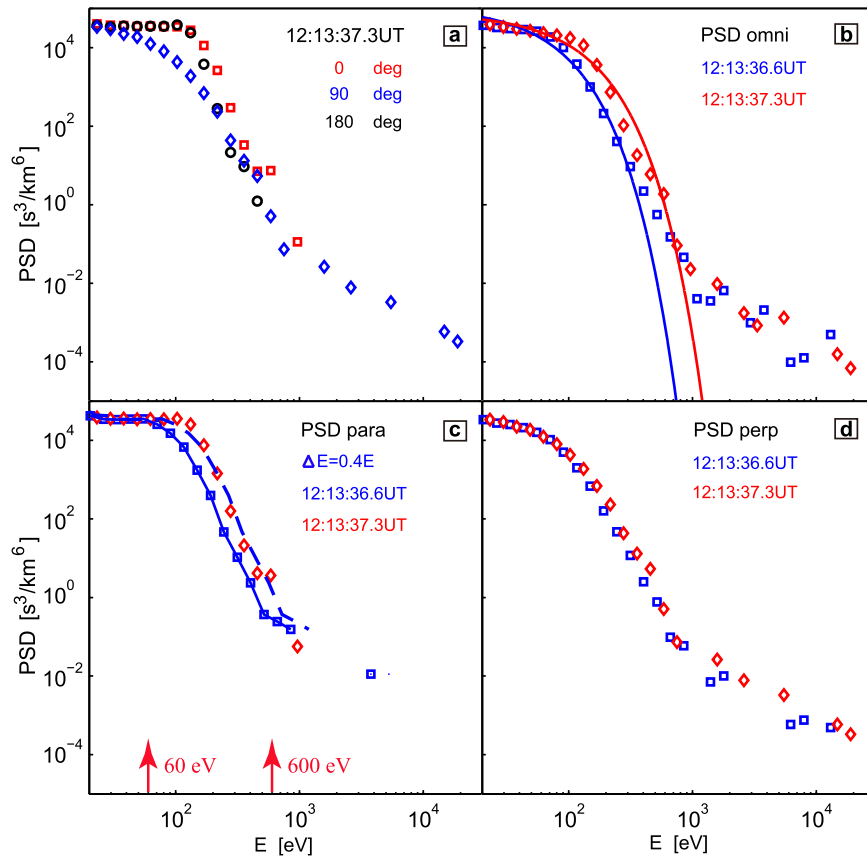


**Figure 3.** Modeling of electron acceleration at the edge of high-speed jet. (a) The phase space density (PSD) of electrons at 12:13:37.3 UT in the parallel, perpendicular, and antiparallel directions, (b)–(d) the PSD of electrons at 12:13:36.6 and 12:13:37.3 UT in the omni-, parallel, and perpendicular directions. In (b), the solid lines are fittings of the PSDs by the Maxwellian distributions; in (c), the dashed line is the modeling result of electron acceleration based on Liouville’s theorem. The diamonds represent different directions in (a) but different times in (b)–(d).

parallel direction—as shown by the big discrepancy between the two parallel PSDs in Figure 3(c), but does not happen in the perpendicular direction—because the perpendicular PSDs of these two populations are almost the same (see Figure 3(d)).

We can use a simple model to reproduce the heating process in the framework of Liouville’s theorem, which requires the PSD to be a constant during acceleration (Egedal et al. 2010; Liu et al. 2017a, 2017b; Fu et al. 2019c). Specifically, we treat the electron population at 12:13:36.6 UT as the source (blue squares in Figure 3(c)), and then move the distribution function of the source (blue solid line in Figure 3(c)) along a constant PSD (Liouville’s theorem) rightward to achieve the energization. We find that the adiabatic energization, with energy uniformly enhanced by 0.4 times ( $\delta E/E = 0.4$  at all energy channels), can make the modeling result (blue dashed line in Figure 3(c)) agree well with the heated electrons measured inside the edge (red diamonds in Figure 3(c)). Therefore, we conclude that the electron heating associated with the TD in this event is caused by the adiabatic energization in the parallel direction. Such adiabatic parallel energization is traditionally referred to as the Fermi process. However, to make sure that the Fermi process can happen, electrons must be trapped and rebounded between two approaching mirror points (Wang et al. 2019).

Figure 4—a close-up view of the TD from 12:13:30 to 12:13:55 UT—demonstrates such possibilities. Specifically, the magnetic field strength, plasma density, electron temperature, electron transverse velocity, PADs of the 0.2–2 and

0.01–0.2 keV electrons, and schematic illustration of the energization process are presented. As can be seen, inside the edge (TD), parallel electron energization—caused by the Fermi process—only occurs during 12:13:37.0–12:13:39.8 UT, 12:13:40.8–12:13:46.0 UT, and 12:13:48.8–12:13:50.2 UT (see the vertical gray shades in Figure 4(c)). Such energization, interestingly, has nice correlation with the plasma density (Figure 4(b)) and anticorrelation with the magnetic field strength (Figure 4(a)): when plasma density increases and magnetic field weakens, the energization appears; when plasma density decreases and magnetic field enhances, the energization disappears. Quite possibly, the magnetic field weakening and density increase are an indication of the magnetic mirror structure (Huang et al. 2017a, 2017b; Yao et al. 2017, 2018; Liu et al. 2019). Indeed, the HSJ wrapped by the TD provides a condition for producing such a magnetic mirror structure, as shown in Figures 4(g)–(h). Here Figure 4(g) corresponds to the small transverse section (in  $L$ – $N$  plane) of the jet in Figure 2(a), while Figure 4(h) corresponds to the large transverse section of the jet in Figure 2(a) (the coordinates in Figures 4(g)–(h) and Figure 2(a) are the same). We can use the model in Figures 4(g)–(h) to interpret the formation of such mirror-mode structure, by considering that the transverse section of the HSJ is time-varying (see Figure 2(a)). Such a model can be described as follows.

When the transverse section of the HSJ decreases, as in the case in Figure 4(g), the magnetic field near the HSJ (at P2) is not compressed, and consequently, no magnetic mirror

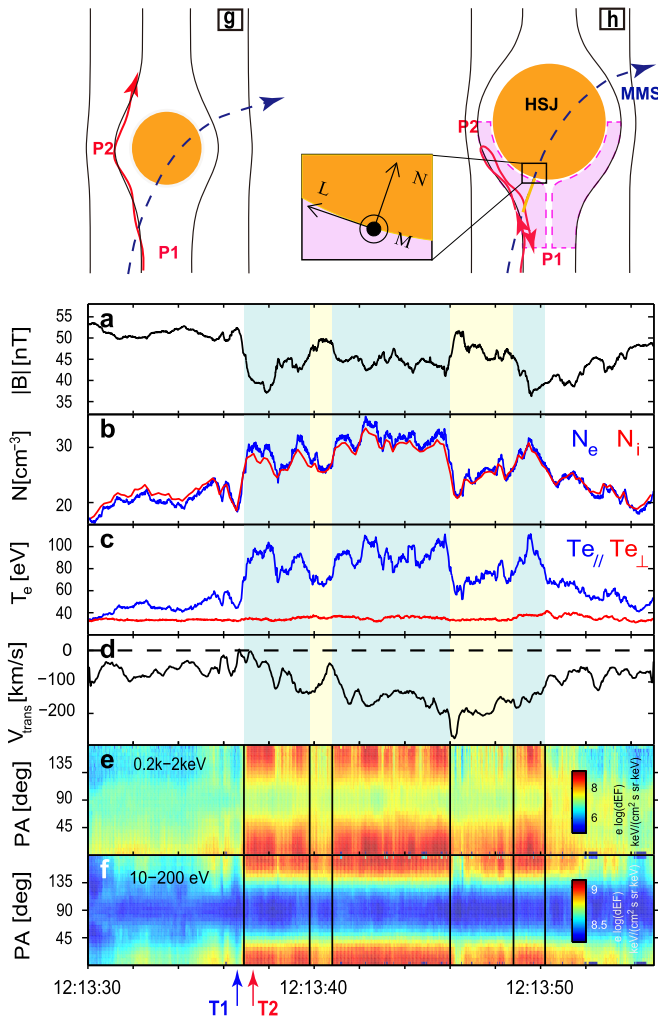


**Figure 4.** Explanation of the parallel electron acceleration in this event. (a) Magnetic field magnitude; (b) the plasma density; (c) the electron temperature; (d) the transverse velocity of electrons relative to the HSJ; (e)–(f) the pitch angle distribution of the 0.2–2 and 0.01–0.2 keV electrons; (g)–(h) a model demonstrating the formation of magnetic mirror and the energization process.

structure is formed in this case, which means that electrons can move freely along the magnetic field line without reflection and trapping (see the red arrow in Figure 4(g)). This can explain the low electron flux and plasma density measured by MMS (see the vertical yellow shades in Figures 4(a)–(f)), because electrons are not trapped in such a situation.

When the transverse section of the HSJ increases, as in the case in Figure 4(h), the magnetic field near the HSJ (at P2) is significantly compressed, and consequently, a magnetic mirror structure is formed at the edge of the HSJ (see the pink area in Figure 4(h)). Due to the existence of such a magnetic mirror, electrons cannot move freely along the magnetic field line. Instead, they will be reflected and trapped inside the mirror-mode structure (see the red arrow in Figure 4(h)). If a spacecraft crosses the central part of this structure (see the orange line in Figure 4(h)), it certainly measures the cigar-type distribution of electrons. Interestingly, during the gradual increase of the transverse section of the HSJ, the mirror point P2 will be squeezed to move toward mirror point P1, which results in the Fermi acceleration of electrons. This can explain the high electron flux and plasma density measured by MMS (see the vertical gray shades in Figures 4(a)–(f)). Moreover, the

expansion of the HSJ has a timescale of 1.4–5.2 s (see the blue shades), which is about 1.1–4.2 ion cyclotron periods. Considering that the average pulsation speed of the TD is  $18.3 \text{ km s}^{-1}$  (from timing analysis), the pulsation has a spatial scale of  $\sim 95 \text{ km}$  in 5.2 s, which is about  $1.6 d_i$ . Interestingly, the observed TD pulsation speed supports our interpretation of the electron heating. Consider a particle with velocity  $V$  moves toward a head-on collision with the mirror point P2 moving at velocity  $W$ . By transforming into and out of the frame of the mirror point, one can see that the energy gain  $\Delta E$  of the particle is  $\frac{\Delta E}{E} = 4 \times \frac{W}{V}$ . Considering that the tangential flow velocity is  $V \approx 140 \sim 180 \text{ km s}^{-1}$  (Figure 2(e)) and the energy gain is  $\frac{\Delta E}{E} \approx 0.4$  (Figure 3(c)), we can obtain the velocity of the mirror point P2 as  $W \approx 14 \sim 18 \text{ km s}^{-1}$ . This result agrees well with the observed TD pulsation speed by assuming that the mirror point P2 moves with the TD when the HSJ expands.




Therefore, according to these analyses, the time-varying HSJ indeed can lead to the Fermi acceleration of electrons and consequently the parallel-temperature increase at the TD. The transverse velocity of electrons (Figure 4(d)), which is approximately the transverse velocity of magnetic structures because of the magnetization of electrons, indicates an expansion of the HSJ ( $|V_{\text{trans}}|$  increase, see the gray shades in Figure 4(d)) during the Fermi acceleration and a contraction of the HSJ ( $|V_{\text{trans}}|$  decrease, see the yellow shades in Figure 4(d)) during the escape of electrons. This qualitatively supports our proposition that the parallel electron heating in this event is caused by the time-varying size of the HSJ. Unfortunately, it is difficult to verify this proposition quantitatively, owing to the lack of a precise model describing the magnetic mirror structure. Moreover, it seems that our scenario does not work well in the third gray shade (see Figures 4(a)–(f)). This is probably because the transverse velocity  $|V_{\text{trans}}|$  during that period has no clear trend (neither increases dramatically nor decreases dramatically).

### 3. Conclusions

In summary, we report significant electron energization at the edge of a high-speed jet (HSJ) in the turbulent magnetosheath, which is identified as a tangential discontinuity (TD) in the MHD regime but exhibits fine structures in the kinetic-scale regime. We find that the energization is primarily in the direction parallel to magnetic field and results in three times of parallel-temperature increase. We propose a model to interpret such parallel heating based on the time-varying size of the HSJ: when the transverse section of the HSJ increases, a magnetic mirror is formed and subsequently electrons are trapped and accelerated via the Fermi mechanism; when the transverse section of the HSJ decreases, the magnetic mirror disappears and subsequently electrons escape. This study, for the first time showing electron heating/energization by the TD, can shed light on the study of electron heating in the solar wind, where TDs exist extensively.

We thank the MMS Science Data Center (<https://lasp.colorado.edu/mms/sdc/public/>) for providing the data for this study. This research was supported by NSFC grants 41404133, 41874188, 41574153, 40621003, and 41431071.

## ORCID iDs

H. S. Fu  <https://orcid.org/0000-0002-4701-7219>  
 C. M. Liu  <https://orcid.org/0000-0002-9705-5387>  
 Z. Wang  <https://orcid.org/0000-0002-1720-964X>

## References

- Agapitov, O. V., Artemyev, A. V., Mourenas, D., et al. 2014, *JGRA*, **119**, 1606  
 Amata, E., Savin, S. P., Ambrosino, D., et al. 2011, *P&SS*, **59**, 482  
 Burch, J. L., Moore, T. E., Torbert, R. B., & Giles, B. L. 2016, *SSRv*, **199**, 5  
 Cairns, I. H., & McMillan, B. F. 2005, *PhPI*, **12**, 102110  
 Cao, D., Fu, H. S., Cao, J. B., et al. 2017, *GeoRL*, **44**, 3954  
 Chasapis, A., Matthaeus, W. H., Parashar, T. N., et al. 2017, *ApJ*, **836**, 247  
 Chasapis, A., Retinò, A., Sahraoui, F., et al. 2015, *ApJL*, **804**, L1  
 Chen, X. H., Fu, H. S., Liu, C. M., et al. 2018, *ApJ*, **852**, 17  
 Cohen, I. J., Mauk, B. H., Anderson, B. J., et al. 2016, *GeoRL*, **43**, 5960  
 Dmitriev, A. V., & Suvorova, A. V. 2012, *JGR*, **117**, A08217  
 Drake, J. F., Swisdak, M., Che, H., & Shay, M. A. 2006, *Natur*, **443**, 553  
 Duan, A. Y., Cao, J. B., Dunlop, M., & Wang, Z. Q. 2014, *JGRA*, **119**, 8902  
 Egedal, J., Lê, A., Zhu, Y., et al. 2010, *GeoRL*, **37**, L10102  
 Eriksson, E., Vaivads, A., Graham, D. B., et al. 2016, *JGRA*, **121**, 9608  
 Eriksson, E., Vaivads, A., Graham, D. B., et al. 2018, *GeoRL*, **45**, 8081  
 Fu, H. S., Cao, J. B., Cao, D., et al. 2019a, *GeoRL*, **46**, 48  
 Fu, H. S., Cao, J. B., Khotyaintsev, Y. V., et al. 2013a, *GeoRL*, **40**, 6023  
 Fu, H. S., Cao, J. B., Mozer, F. S., et al. 2012a, *JGRA*, **117**, A01203  
 Fu, H. S., Cao, J. B., Yang, B., & Lu, H. Y. 2011a, *JGR*, **116**, A10210  
 Fu, H. S., Cao, J. B., Zong, Q. G., et al. 2012b, *JASTP*, **80**, 37  
 Fu, H. S., Khotyaintsev, Y. V., André, M., & Vaivads, A. 2011b, *GeoRL*, **38**, L16104  
 Fu, H. S., Khotyaintsev, Y. V., Vaivads, A., et al. 2012c, *JGR*, **117**, A12221  
 Fu, H. S., Khotyaintsev, Y. V., Vaivads, A., et al. 2012d, *GeoRL*, **39**, L06105  
 Fu, H. S., Khotyaintsev, Y. V., & Vaivads, A. 2013b, *NatPh*, **9**, 426  
 Fu, H. S., Peng, F. Z., Liu, C. M., et al. 2019b, *GeoRL*, **46**  
 Fu, H. S., Vaivads, A., Khotyaintsev, Y. V., et al. 2017, *GeoRL*, **44**, 37  
 Fu, H. S., Xu, Y., Vaivads, A., & Khotyaintsev, Y. V. 2019c, *ApJL*, **870**, L22  
 Gabrielse, C., Angelopoulos, V., Runov, A., & Turner, D. L. 2014, *JGRA*, **119**, 2512  
 Guo, F., Li, H., Daughton, W., & Liu, Y. H. 2014a, *PhRvL*, **113**, 155005  
 Guo, X., Sironi, L., & Narayan, R. 2014b, *ApJ*, **794**, 153  
 Han, D. S., Hietala, H., Chen, X. C., et al. 2017, *JGRA*, **122**, 1853  
 Hietala, H., Laitinen, T. V., Andréová, K., et al. 2009, *PhRvL*, **103**, 245001  
 Hietala, H., Phan, T. D., Angelopoulos, V., et al. 2018, *GeoRL*, **45**, 1732  
 Hoshino, M. 2012, *PhRvL*, **108**, 135003  
 Huang, S. Y., Du, J. W., Sahraoui, F., et al. 2017a, *JGRA*, **122**, 8577  
 Huang, S. Y., Sahraoui, F., Yuan, Z. G., et al. 2017b, *ApJL*, **836**, L27  
 Hughes, R. S., Gary, S. P., & Wang, J. 2014, *GeoRL*, **41**, 8681  
 Johlander, A., Schwartz, S. J., Vaivads, A., et al. 2016, *PhRvL*, **117**, 165101  
 Liu, C. M., & Fu, H. S. 2019, *ApJL*, **873**, L2  
 Liu, C. M., Fu, H. S., Cao, J. B., et al. 2017a, *GeoRL*, **44**, 10116  
 Liu, C. M., Fu, H. S., Vaivads, A., et al. 2018a, *GeoRL*, **45**, 556  
 Liu, C. M., Fu, H. S., Xu, Y., et al. 2017b, *GeoRL*, **44**, 6492  
 Liu, C. M., Fu, H. S., Xu, Y., et al. 2017c, *JGRA*, **122**, 594  
 Liu, C. M., Fu, H. S., Xu, Y., et al. 2018b, *GeoRL*, **45**, 4628  
 Liu, H., Zong, Q. G., Zhang, H., et al. 2019, *NatCo*, **10**, 1040  
 Matsumoto, Y., Amano, T., Kato, T. N., & Hoshino, M. 2015, *Sci*, **347**, 974  
 Oka, M., Wilson, L. B., III, Phan, T. D., et al. 2017, *ApJL*, **842**, L11  
 Palmroth, M., Hietala, H., Plaschke, F., et al. 2018, *AnGeo*, **36**, 1171  
 Park, J., Caprioli, D., & Spitkovsky, A. 2015, *PhRvL*, **114**, 085003  
 Peng, F. Z., Fu, H. S., Cao, J. B., et al. 2017, *JGRA*, **122**, 6349  
 Peng, I. B., Markidis, S., Laure, E., et al. 2015, *PhPI*, **22**, 092109  
 Phan, T. D., Eastwood, J. P., Shay, M. A., et al. 2018, *Natur*, **557**, 202  
 Plaschke, F., Hietala, H., & Angelopoulos, V. 2013, *AnGeo*, **31**, 1877  
 Pollock, C., Moore, T., Jacques, A., et al. 2016, *SSRv*, **199**, 331  
 Retinò, A., Sundkvist, D., Vaivads, A., et al. 2007, *NatPh*, **3**, 235  
 Russell, C. T., Anderson, B. J., Baumjohann, W., et al. 2016, *SSRv*, **199**, 189  
 Sundkvist, D., Retinò, A., Vaivads, A., & Bale, S. D. 2007, *PhRvL*, **99**, 025004  
 Torbert, R. B., Russell, C. T., Magnes, W., et al. 2016, *SSRv*, **199**, 105  
 Turner, D. L., Claudepierre, S. G., Fennell, J. F., et al. 2015, *GeoRL*, **42**, 2079  
 Wan, M., Matthaeus, W. H., Karimabadi, H., et al. 2012, *PhRvL*, **109**, 195001  
 Wang, B., Nishimura, Y., Hietala, H., et al. 2018, *JGRA*, **123**, 4879  
 Wang, Z., Fu, H. S., Liu, C. M., et al. 2019, *GeoRL*, **46**, 1195  
 Wilson, L. B., III, Koval, A., Szabo, A., et al. 2013, *JGRA*, **118**, 5  
 Xu, Y., Fu, H. S., Liu, C. M., & Wang, T. Y. 2018, *ApJ*, **853**, 11  
 Yao, S. T., Shi, Q. Q., Liu, J., et al. 2018, *JGRA*, **123**, 5561  
 Yao, S. T., Wang, X. G., Shi, Q. Q., et al. 2017, *JGRA*, **122**, 1990  
 Yordanova, E., Vörös, Z., Varsani, A., et al. 2016, *GeoRL*, **43**, 5969  
 Zank, G. P., Hunana, P., Mostafavi, P., et al. 2015, *ApJ*, **814**, 137  
 Zhao, M. J., Fu, H. S., Liu, C. M., et al. 2019, *GeoRL*, **46**, 2390  
 Zong, Q. G., Wang, Y. F., Zhang, H., et al. 2012, *JGR*, **117**, A11206  
 Zong, Q. G., Zhou, X. Z., Wang, Y. F., et al. 2009, *JGR*, **114**, A10204